Linking Methane Seepage to Fluid Flow Mechanisms: Evidence from AVO Characteristics of Bottom Simulating Reflectors

Sanjeev Rajput[a],*; N. K. Thakur[b]; P. Prasada Rao[b]

[a]Commonwealth Scientific and Industrial Research Organization (CSIRO), Earth Science and Resource Engineering, 26 Dick Perry Ave, Kensington, Perth, Western Australia 6151.
[b]Council of Scientific and Industrial Research (CSIR), National Geophysical Research Institute, Uppal Road, Hyderabad, India.
* Corresponding author.

Abstract

The presence of gas hydrates over continental margins may be inferred by various seismic indicators, including the bottom simulating reflector (BSR). Recently, the occurrence of two BSRs have been reported from many regions of the world. In this study we estimate the uncertainty in amplitude versus offset (AVO) behaviour of the single BSR and double bottom simulating reflector (DBSR) observed over two geological provinces; the Kerala-Konkan Basin, offshore India and Green Canyon, offshore USA, and attempt to infer a mechanism for the observed anomalies from the AVO patterns. Anomalous behaviour of seismic velocities within the gas hydrate stability zone (GHSZ) associated with the occurrence of DBSRs, low amplitude seismic chimneys and bright spots, indicates increased hydrate concentration and fluid venting structures underneath the DBSR locations. Such structures, if extended upward into the regional GHSZ through discrete fracture networks, may act as a passage for methane escape into the ocean. Our analysis indicates that the variability in AVO signatures for gas hydrate saturated sediments is potentially linked to the discrete zones of steeply inclined fractures that are responsible for the migration of deep gas and its escape through the seabed.

Key Words: Methane hydrate; Gas dynamics; Seismic reflections; Plumbing system; Amplitude versus offset (AVO); Bottom simulating reflector

INTRODUCTION

Methane hydrate is a class of clathrate, composed of water and low molecular weight gases, mainly methane, which forms under low temperature, high pressure, and appropriate methane concentrations. Hydrates with free-gas beneath them form a strong acoustic interface, which is often conspicuous in seismic sections as bright reflections known as bottom simulating reflectors (BSRs). These are interpreted as the primary geophysical indicator for inferring the presence of gas hydrate (Andreassen *et al*., 1990; Shipley *et al*., 1979). The BSR corresponds to a thermodynamic phase boundary at the base of the hydrate stability zone (HSZ), a region that includes the uppermost several hundred metres of sediment where low temperatures and high pressures force the excess methane dissolved in pore water to form hydrates (Gorman *et al*., 2002). A BSR is identified on multi-channel or multi-component (4C) seismic sections as a high amplitude seismic reflection that mimics the sea floor reflection but with inverse polarity. As the BSR is a thermodynamic phase boundary it may cross cut the bedding plane of sedimentary layers (Hyndman and Spence, 1992; Thakur and Rajput, 2010). The ice-like structure of gas hydrate consists of light hydrocarbons (mostly methane) trapped by a rigid cage of water molecules.

Gas hydrates occur naturally in the pore space of sediments when appropriate high pressure and low temperature conditions exist (Sloan, 1998). These

conditions confine gas hydrates to the upper few hundred metres of sediments, the gas hydrate stability zone (GHSZ). Pure gas hydrate has a high P-wave velocity (3000 m/s), and therefore sediments partially saturated with hydrate are characterized by higher velocities than brine saturated sediments (Ecker, Dvorkin and Nur, 1998). The presence of hydrates in the pore space reduces porosity and permeability of the sediment, and they typically form a partial hydrological seal for upward migrating fluid and gas (Nimblett and Ruppel, 2003). The BSR is characterized by increase in negative amplitude with increasing offset i.e. the compressional velocity above the BSR is larger than that below BSR (Ecker *et al.*, 1998). Hence, if only a small percentage of free gas exists below the GHSZ, the P-wave velocity there may sharply decrease to below the acoustic velocity of water i.e., 1475 m/s (Ecker *et al.*, 1998). The velocity reversal occurs at BSR which delineates the base of GHSZ, and allows the determination of gas hydrate without drilling. Below the BSR, the hydrate destabilizes, so that in methane-saturated pore fluids, additional methane is in gas form and is considered as free gas (Buffett and Zatsepina, 1999).

In recent times the occurrence of DBSRs have been identified on seismic reflection sections (Posevang and Mienert, 1999; Bangs, Musgrave and Trehu, 2005; Rajput *et al.*, 2010). Trehu *et al.* (1999) suggested that DBSR at Hydrate Ridge, offshore USA, is caused by tectonic uplifting, growth of an anticline structure, sea level change, or a change in the water bottom temperature. Bangs, Musgrave and Trehu (2005) made a case for interpreting the DBSR as a relic of the glacial GHSZ. Below a certain depth, depending on the local temperature conditions, hydrates cannot form, and only free methane exists. Gas Hydrates are found to occur in the depth range between sea floor and base of hydrate stability zone (BHSZ)/top of free gas zone. Musgrave *et al.* (2006) suggested that slow migration of the base of gas hydrate stability zone (BGHSZ) in the closing stages of the last glacial period allowed accumulation of free methane below the hydrate zone. This established a rock magnetic signal that has survived the subsequent rapid upward movement of the BGHS as the pulse of heat from water bottom warming reset the geothermal profile over Hydrate Ridge. Recently, the thermal nature of the DBSR has been studied (Golmshtok and Soloviev, 2006). With little information available about the DBSRs and lack of suitable models for the interpretation, their formation mechanism is still subject to speculation.

The characteristics of BSRs and DBSRs may vary in a study area and even on a single seismic profile (Rajput *et al.*, 2010). During the past two decades, Amplitude Versus Offset (AVO) techniques have been used for direct detection of gas reservoirs (Ostrander, 1984; Castagna and Backus, 1993; Santoso *et al.*, 1995). For complex geological structures, AVO responses can considerably

reduce uncertainty when predicting the hydrocarbon reserves. Seismic reflection amplitudes that change with offset or incidence angle can be analysed in terms of the reflection coefficient characteristics. For isotropic media Zoeppritz (1919) produced a set of equations to compute the particle displacement amplitude of reflected and transmitted waves. In the presence of anisotropy, the behaviour of elastic waves becomes more complicated and required sophisticated analysis techniques (Rueger, 1996; Tsvankin, 2005; Behura and Tsvankin, 2009). Here we use the formulation proposed by Rueger (1996) to derive the reflection coefficient of the BSR for both synthetic and real data.

Gas hydrate provinces are associated with methane gas seepage in both passive and active margin settings (Holbrook *et al.*, 2002). Structures for hydrocarbon accumulation and structural pathways (faults and fractures) for fluid migration are important factors contributing to the presence of methane seepage. In low permeability environments, vertically focused fluid-flow is generally initiated through the process of natural hydraulic fracturing (Morley, 2003; Tingay *et al.*, 2003; Zuhlsdorff and Spiess, 2004). Conventional seismic analyses typically reveal these venting structures as near-vertical, well-defined distorted columns of seismic 'wipe-out' (loss of coherency), and are termed seismic chimneys or pipes (Heggland, 1997; Løseth *et al.*, 2001).

Here we attempt to model BSR from Kerala-Konkan basin (K-K), offshore Indian margin and a Double BSR (DBSR) from Green Canyon (GC), Gulf of Mexico (GoM), offshore USA and try to arrive at the probable cause of observed geophysical signatures. We evaluate the amplitude versus offset (AVO) characteristics and compare the reflection coefficient behaviour for real and modelled BSRs. We use real anisotropy parameters from other comparable regions such as Blake ridge, (Peacher *et al.*, 2003) and model the reflection coefficient variability of gas hydrate related reflectors. Notably, our analysis indicates that the variability in AVO signatures for gas hydrate saturated sediments is potentially linked to discrete zones of steeply inclined fractures that are responsible for the migration of deep gas and its escape through the seabed.

1. GEOLOGICAL DESCRIPTION AND SEISMIC INTERPRETATION

Methane hydrates can be found in the shallow sediments of many deep ocean areas. The clathrate itself forms an impermeable thin high-velocity layer, and below this, we sometimes see an accumulation of free gas, giving rise to a low-velocity zone immediately below the high-velocity clathrate layer. These form zones which strongly attenuate seismic amplitudes and are characterized by strong reflectivity due to the higher-velocity hydrates overlying

the lower-velocity free gas interval. Dim zones occur beneath these gas hydrate pockets. The size and shape of the dim zones vary over different offsets. The analyses of seismic data from KK basin suggest that the dimming anomalies are present (Figure 1) in the region and represent deformation irrespective of presence of free gas or not. Figure 1 shows the BSR observed on the seismic section from KK basin exhibits the reverse polarity and stronger seismic amplitude for hydrate saturated sediments than for equivalent water saturated sediments. Hydrate recycling and vertical migration of fluids from deep sources are processes evoked as controllers of the formation and stability of the free gas zone (FGZ) beneath the base of the gas hydrate stability zone (BGHSZ).
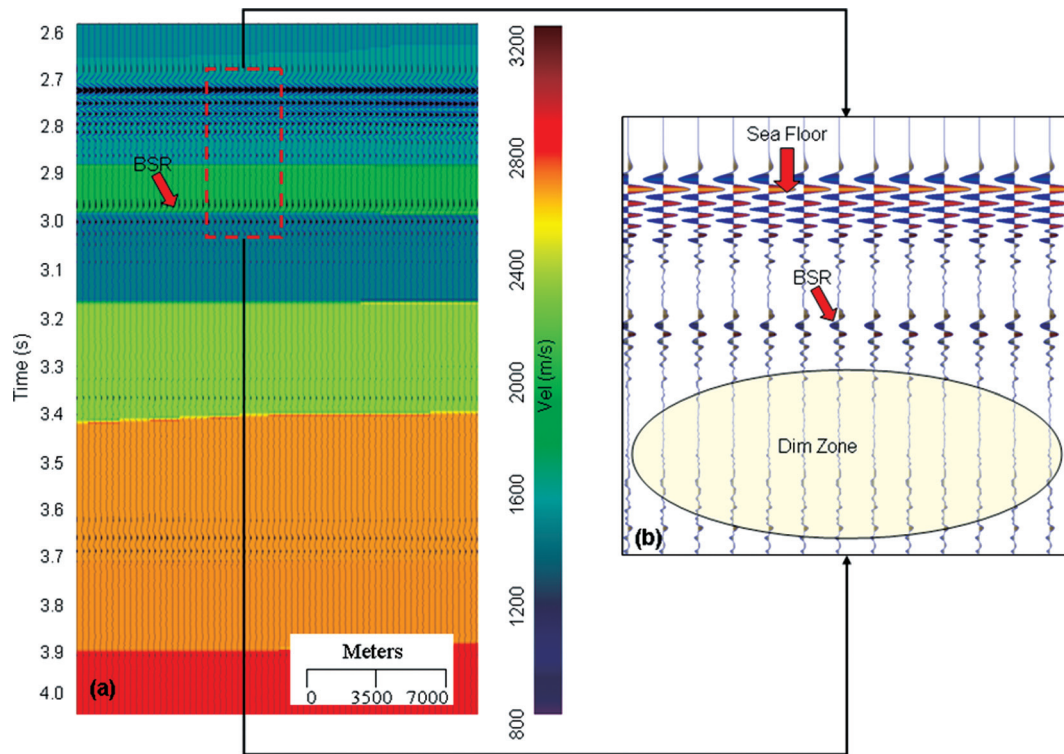
Figure 1
Example from KK Basin
(a) Migrated seismic image of a part of the KK basin is superimposed on the seismic stacking velocities. Different colours represent variations in velocities. At 3.0 s, a BSR is identified as a reverse polarity event and marked. (b) Zoomed in part of the red dotted box of (a). The sea floor and BSR show reverse polarity. Weak amplitudes are seen in the zone referred to as dim zone.

The seismic data from GC (Figure 2) show a 'leaky' gas hydrate province (labeled as 'A', 'B' and 'C' in Figure 2) in which tectonically controlled structural elements promote the rapid migration of thermogenic gas from sub-seabed reservoirs to the sea floor. Localized amplitude dimming with seismic pull up and mound-like features are observed. In typical gas hydrates, mound-like structures form when the proper temperature, pressure and chemical composition for the gas are achieved (feature 'A' in Figure 2). The apparent gas migration pathways (seismic chimney) and funneling of deep gases into the base of vent feature B suggest a high gas flux into this vent. A high upward flux of gas would also account for the large velocity anomaly due to the hydrate accumulation in the vent.

The DBSR observed at feature 'C' (Figure 2) is caused by a low velocity layer (LVL) lying within the GHSZ as shown in Figure 2b. This LVL is probably caused by the structural elements (gas vent structures, faults, folds, mounds, fractures etc.) present in the GC region (Gorman *et al*., 2002). The seepage of methane could be from destabilization of gas hydrates or free gas through structural elements such as faults and fractures or could be from a gas-bearing source rock by filtration and diffusion processes (Zuhlsdorff and Spiess, 2004). Within feature 'C' (Figure 2), the permeable pathways locally connect the free gas zone to the sea floor. This occurs where the impermeable cap of young, un-faulted and un-fractured sediments has been removed by erosion or breached by gently dipping sediments, where on-lapping sediments will guide fluid flow. Seismically similar features have been investigated from a variety of geographic areas, including the Niger Delta (Hovland *et al*., 1997), Norwegian margin (Hovland and Svensen, 2006), Blake Ridge (Paull *et al*., 1995), the Cascadia margin (Suess *et al*., 1999; Riedel *et al*., 2006) and offshore Korea (Haacke *et al*., 2009).
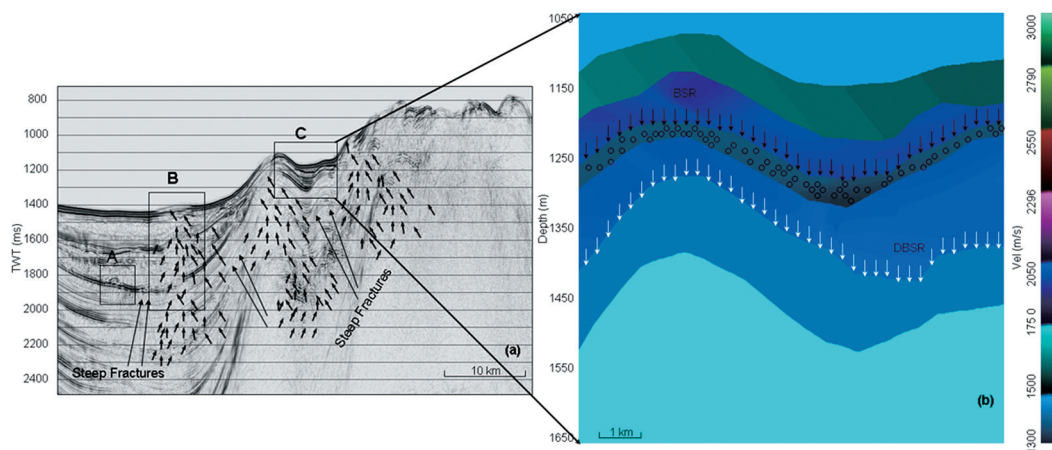
Figure 2
Time Migrated Section from the GC Region, Offshore USA and Velocity Model for Around the DBSR
(a) Three structures (labelled 'A', 'B' and 'C') are discussed in the text below ('interpretation'). Long arrows indicate near vertical fractures. Small arrows show the migration of gas from deeper in the section to the seabed. **(b)** Seismic velocity model of the feature 'C' in 'Figure 2a'. Black arrows represent the location of the BSR and white arrows show the location of the DBSR. Black circles show the accumulation of fluids and gas within the GHSZ.

Close inspection of the migrated seismic images (Figure 3) shows that the vertical vent (seismic chimney) is composed of steep amplitude striations that are probably swarms of cracks and fractures that are described by (Haacke *et al.*, 2009; Zuhlsdorff and Speiss, 2004). The seismic pull-up of BSR around and beneath at hydrate mound (feature 'A' in Figure 2 that corresponds to Figure 3a), could indicate some degree of upward bending of the GHSZ due to warm upwelling fluids as suggested by Wood *et al.*, (2002). The gas hydrates at hydrate mounds are not dispersed in sediments as nodules or thin seams, but instead occur as continuous masses. Velocity analysis suggests that in this structure there is already a high concentration of hydrate and rapid migration of gas through these sediments resulted in the disruption of the stratal relationship that give the surrounding rock its reflective character. The incoherent reflections at feature B (Figure 2 and Figure 3b) indicate the focusing of lower concentrations of the gas towards the base of seismic chimney, which carries the gas through the sea floor and into the overlying ocean. Fluid flow is very important in the formation of gas hydrates as it provides a pathway for the movement of fluid from the hydrate. In hydrodynamic environments, although gas usually moves vertically upward due to buoyancy, water may move in any direction (Zhang, Han and Yao, 2011). Thus, fluid migration (including both water and gas) can be vertical along faults, which act as pathways for fluid transport. It also can be horizontal within high permeability sandy sediments. These sandy sediments may act as either pathways or intermediate reservoirs to concentrate fluids (Gay *et al.*, 2007). The apparent gas migration pathways (seismic chimney) and funneling of deep gases into the

base of vent feature B (Figure 2) suggest a high gas flux into this vent. A high upward flux of gas would also account for the large velocity anomaly due to the hydrate accumulation in the vent. In the sediment-filled plain of the GC, a number of buried faults produce a series of surface spots or diffuse gas vents (Gorman *et al.*, 2002; Haacke *et al.*, 2009; Haacke, Westbrook and Hyndman, 2007). Gas flow there was found to be spatially discontinuous and variable in nature. Gas migration pathways ranged from relatively small, high-flux points (due to fault intersections), to more diffuse, low-flux areas (represent large brittle fracture zones).

We observed a possibility of rapid formation of hydrate in the GC region from migrating gas decoupled from upwelling liquid that consumes water while excluding salts. This could change the local stability conditions until hydrate coexists with liquid and gas and free gas can escape through the GHSZ to the ocean. Near the seabed, because of the large salinity gradient, the anomaly could be reduced by upward diffusion, which could enable further formation of hydrate at or near the sea floor. The interpretation shows that the physical characteristics of various gas venting structures control their source and distribution in the subsurface and their eventual linking into the seabed. Gas hydrate in the GC area occurs near the seafloor, indicating that gassy fluids move into the gas hydrate stability zone. Large faults are clearly observed in the study area and one example is shown in Figure 3d. The presence of the fault is very important for the vertical migration of free gas. Vertical gas venting pathways though faults are inferred (Figure 3d). Our interpretation indicates that the fault serves a conduit for gas migration in upward direction.
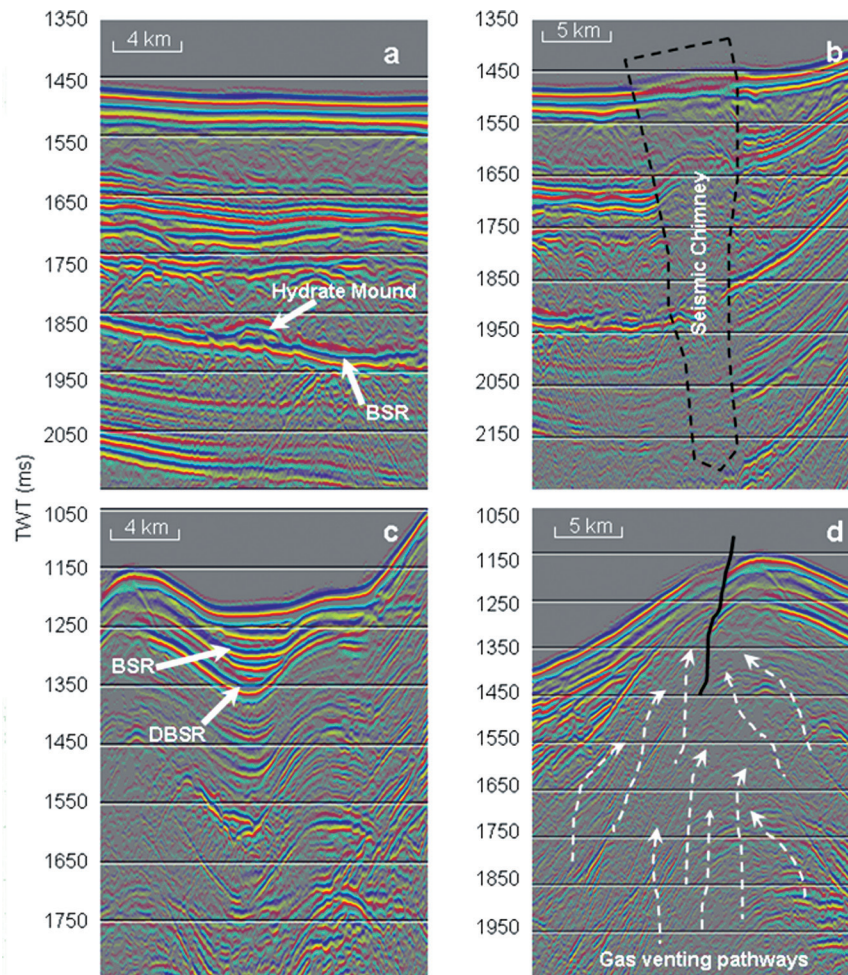
Figure 3
Detailed Seismic Reflection Sections from Three Boxed Areas of Figure 2 and an Observed Steep Fault
Steep amplitude striations in and beneath vent structure 'B' are fractures referred in the text. Seismic pull-up at feature 'A' indicates the accumulation of hydrate as a hydrate mound. At structure 'C', a DBSR is observed. **(a)** Corresponds to feature 'A' in Figure 2. **(b)** Corresponds to feature 'B' in Figure 2, representing a seismic chimney. **(c)** Corresponds to feature 'C' in Figure 2. **(d)** Shows the vertical gas venting pathways though a steep fault from the GC region, GOM, offshore USA. White arrows represent the migration of free gas through this structure as independent feature.
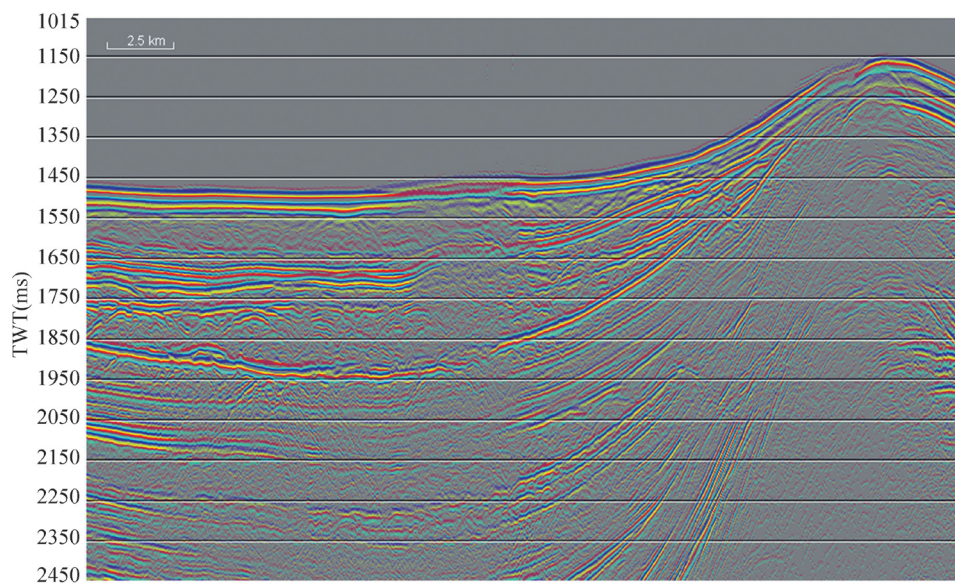
Figure 4
Uninterpreted Time Migrated Seismic Image from a Part of the GC Region, Offshore USA

The uninterpreted (Figure 4) and interpreted seismic sections (Figure 5) indicate that chimneys, consisting of vertical zones of disrupted stratal reflections, appear to be rooted within or below highly reflective strata underneath the BSR. This section from the GC shows that the upper internal amplitude anomalies have apparently positive polarity compared to the seafloor reflection, whereas the lower anomaly shows reversed polarity (indication of a BSR). This may indicate the presence of locally high concentrations of gas hydrate near the seafloor. The internal reflection of the seismic chimney appears highly disrupted. The focused gas flow within the conduits could occur through the cracks initiated by natural hydraulic fracturing (e.g., Morley, 2003). Hydro fracturing may occur when pore pressure exceeds the minimum horizontal stress and the tensile strength of the host sediment (Hubbert and Willis, 1957). Seismic data typically reveal these venting sites as near-vertical distorted zones with low reflectivity, and are termed acoustic chimneys or pipes.
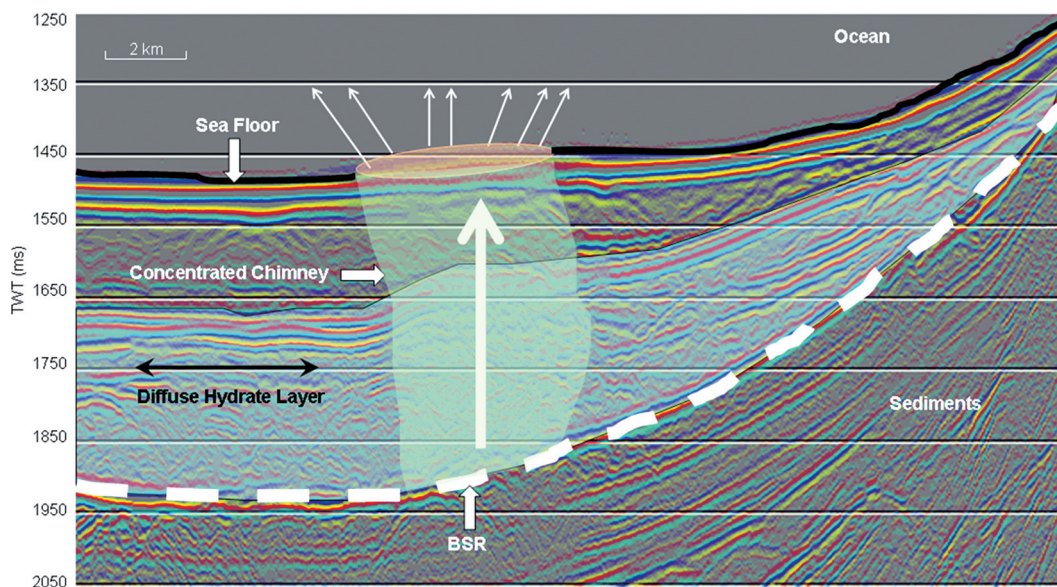
Figure 5
Interpreted Time Migrated Seismic Image from a Part of the GC Region, Offshore USA, this Represents Hydrate Formation and Gas Venting Through Vertical Structures Termed Seismic Chimneys, the Thick White Dashed Line Marks the BSR Which Varies from ~ 1500- 1950 ms TWT

The seismic chimney observed over GC area comprises dimmed reflection with variable continuity. The transition from the dimmed reflections and the outside stratigraphic reflections becomes more diffuse with depth. Therefore it can be said that seismic chimneys, once created, represent long term permeability structure.

2. AVO CHARACTERSTICS

We examine the detailed variation in BSR reflection strength and continuity in order to understand the observed variations in the seismic data for the KK and GC regions. For anisotropic media, the reflection coefficients of the BSR have been estimated by the formulation for P-waves and SV-waves in vertically transverse isotropic (VTI) medium given by Rueger (1996). These equations are good approximations to the exact plane wave reflection coefficients for pre-critical angles of incidence in the context of weak anisotropy. We model the gas hydrate response using velocity estimations from KK basin (Figure 1) and GC basin (Figure 2). In our calculations we include a significant amount of noise to make it comparable to the real data. We focus our analysis on gas hydrate reservoirs with relatively high concentrations of hydrate.

3. MODELLING

The velocities of water and sedimentary layers vary from 1500 m/s to 3200 m/s for the KK basin and the GC region. The velocities of gas hydrates and free gas vary from 1950 m/s - 2060 m/s and 1400 m/s - 1600 m/s respectively. For the single BSR we model the AVO effect using KK basin and GC basin data and for the DBSR we use only GC data. The model parameters correspond to the estimated velocities estimated for the KK (Figure 1) and GC regions (Figure 2). In modelling the VTI case, the velocities of vertically travelling waves differ from horizontal velocities. In the present study we have not considered γ values as this affects only horizontally polarized shear waves. To calculate the reflection coefficient of the BSR in a VTI medium we use the values of anisotropic parameters (ε=0.06 and δ=0.05) for the gas hydrate layer, and (ε=0.17 and δ=0.22) for the free gas layer. These are the typical values obtained for gas hydrates and free gas respectively

from a walkaway vertical seismic profile experiment for the Blake Ridge region (Pecher *et al.*, 2003). First we calculated the reflection coefficient of BSR for real data (GC region from USA and KK basin from offshore India), secondly the reflection coefficients for modeled data for GC and KK basin have been estimated. To this end we plotted the reflection coefficients for real and modelled data for correlation (Figures 6, 7 and 8). Uncertainties (mismatch) in the real and modelled reflection coefficient have been estimated by probability distribution and found under admissible limit.
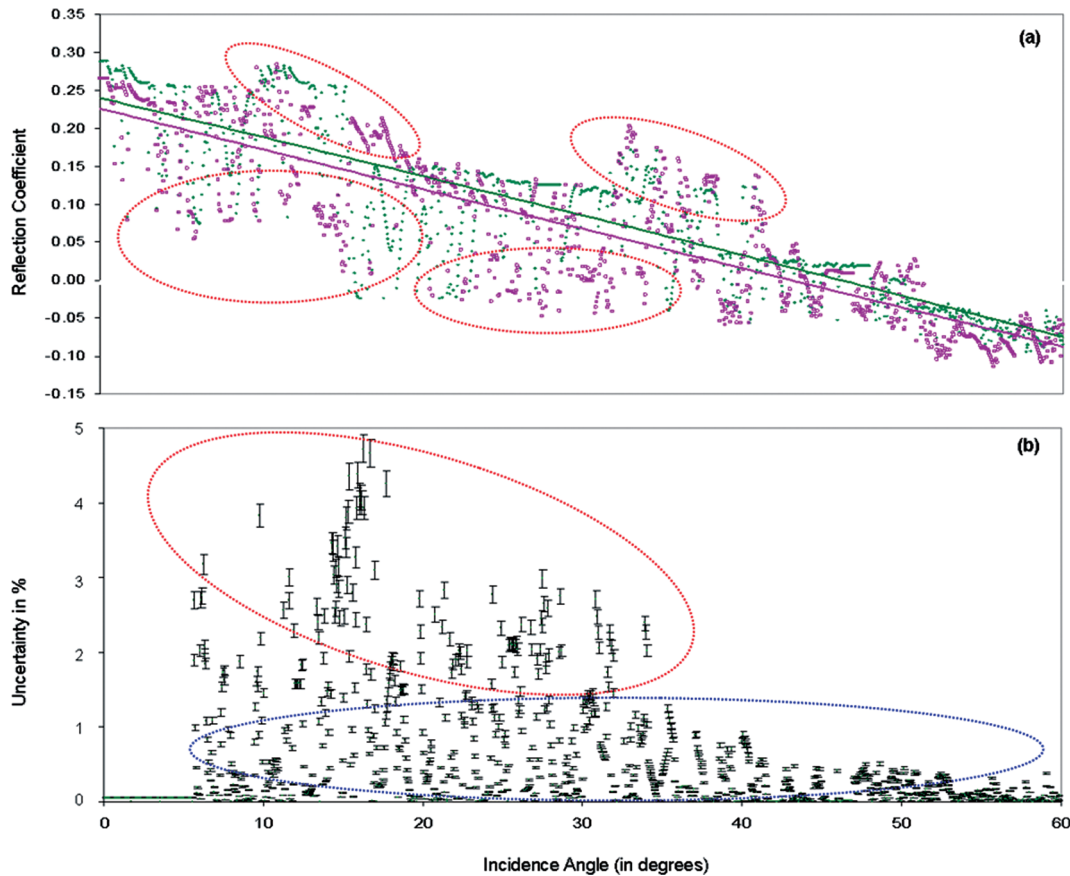
Figure 6
(a)Reflection Coefficient vs. Offset of the Modelled BSR Using the Estimated Seismic Velocities (Pink Dots) and the Real BSR Identified in the KK Basin, Offshore India (Green Dots). The Reflection Coefficients of the Real and Modelled BSR Show a Negative Trend. The Least Square Polynomial Fit for Real (Green Line) and Modelled (Pink Line) Reflection Coefficients of the BSR Correlate Well. Dotted Ovals Show the Scattered Data Points that are Caused by Structural Elements Discussed in the Text;
(b) Estimated Uncertainty by Probability Distribution in the Real and Modelled Values of the Reflection Coefficients of the BSR. The Maximum Uncertainty is 5%. The Blue Dotted Oval Shows that the Majority of Data Points Have less than 2% Uncertainty. The Red Dotted Oval Shows Those Data Points with Uncertainty Between 2% and 5%.

For the KK basin, the two-way traveltimes (TWT) for the observed BSR on one of the seismic lines is around 3.0 s, and the reflection coefficient varies from +0.29 to -0.09. In the KK basin, the amplitude of the BSR varies significantly. This is probably because of wave scattering in the presence of structural elements such as faults, fractures and folds. Supercritical reflection coefficients arise in situations of interest to explorationists. Most AVO approaches using a linearized approximation require incidence angles significantly less than the critical angle. Since the reliability of the estimates is proportional to the range of angles used in the analysis this limits the reliability of the resulting density estimates (Future work).

Large acoustic impedance contrasts between sedimentary strata over the Green Canyon area become problem because the large supercritical reflection coefficients obscure the overlying zone of interest. In this study the AVO analysis of modelled data from the true model parameters with data noise level and incorporating the venting strictures compared with the real data (Figures 6, 7 and 8). These datasets represent the case $V_{p1} > V_{p2}$ (Gas hydrates and free gas), giving the negative reflection coefficients and no critical angle.

The reflection coefficients of the real and modelled BSR correlate well (Figure 6a). The reflection coefficient of the BSR in the KK basin shows decreasing values with

increasing offset, a prognostic indicator of a high-velocity hydrate layer underlain by a low-velocity free-gas layer. Modelling of the KK data shows a maximum uncertainty of about 5%, which is very reasonable; however most of the data points have less than 2% uncertainty (Figure 6b).

In the example from the GC region, offshore USA, the TWT for the first BSR varies from 1200 ms to 1900 ms, and its reflection coefficient (Figure 7a) ranges from -0.10 to -0.90 showing a negative trend with increasing offset. The TWT for the DBSR varies from 1240 ms to 1380 ms. The reflection coefficient of the DBSR varies from -0.16 to - 0.95. The greater scattering in the data compared to the KK data may be attributable to complex

geological and tectonic structural patterns over this region of study. The least square polynomial trend of the BSR reflection coefficients in the GC region vary from -0.10 to -0.50 and from -0.16 to -0.47 for the DBSR. A good polynomial fit between the reflection coefficients of the real and modelled BSRs is observed (Figures 7 & 8). For the first BSR, though most of the data points lie within the accepted limit, the estimated uncertainty is large beyond the critical angle (~ 9% as shown in Figure 7b) and about 4-5% up to the critical angle. For the DBSR case we observed a maximum uncertainty of about 8% (Figure 8b) but most of the data points fall within the acceptable limit.
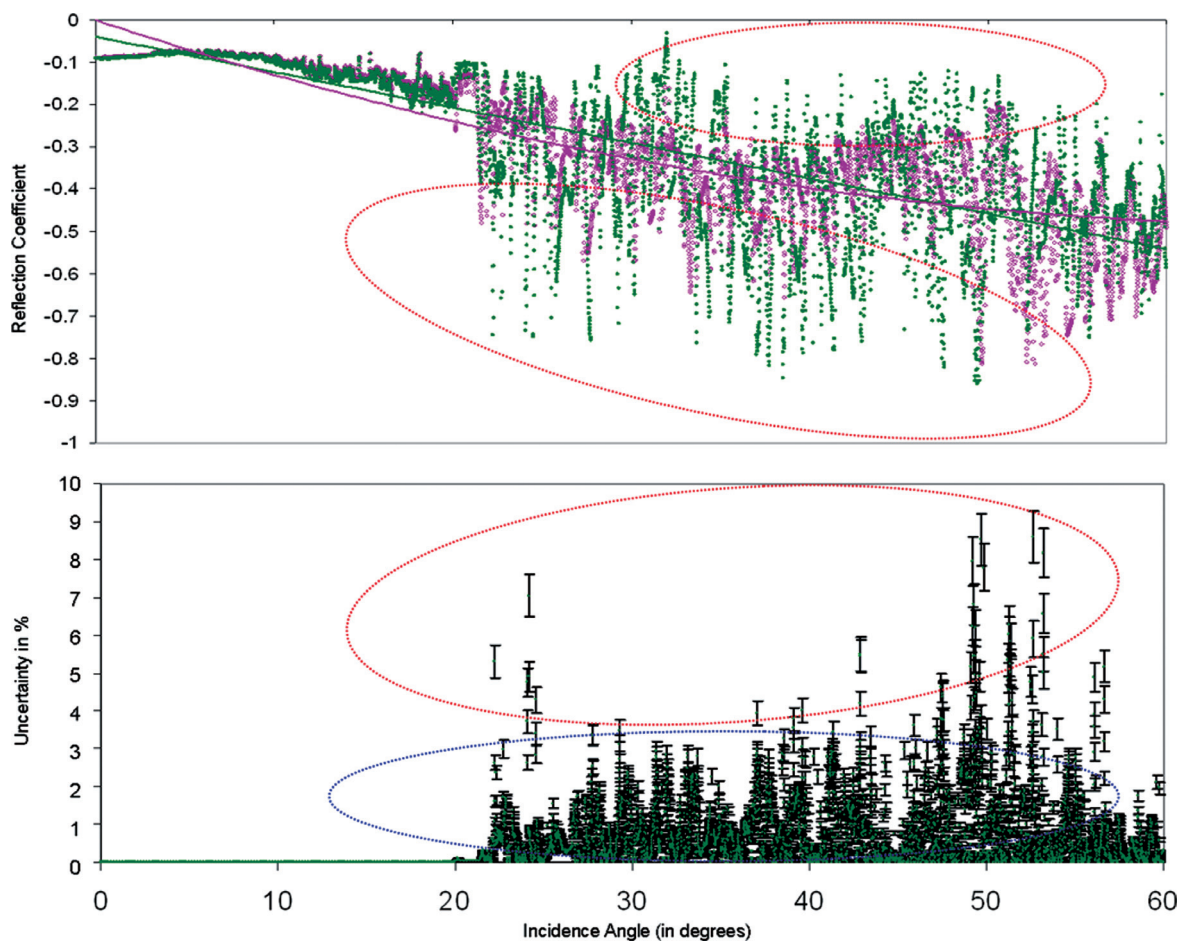
Figure 7
(a) Reflection Coefficient vs. Offset of the Modelled Single BSR (Pink Dots) Using the Estimated Seismic Velocities from Figure 3 and the Real BSR (Green Dots) Identified in GC Region Offshore USA, Showing a Negative Trend. The Least Square Polynomial Fit for Real (Green Line) and Modelled (Pink Line) Reflection Coefficients of the BSR Correlate Well. Dotted Ovals Show the Scattered Data Points that are Caused by Structural Elements Discussed in the Text; **(b) Estimated Uncertainty in the Real and Modelled Values of Reflection Coefficients of the BSR.** The Maximum Uncertainty is 9%. The Blue Dotted Oval Shows that the Majority of Data Points Have Less than 3% Uncertainty. The Red Dotted Oval Shows Those Data Points with Uncertainty Between 3% and 9%.
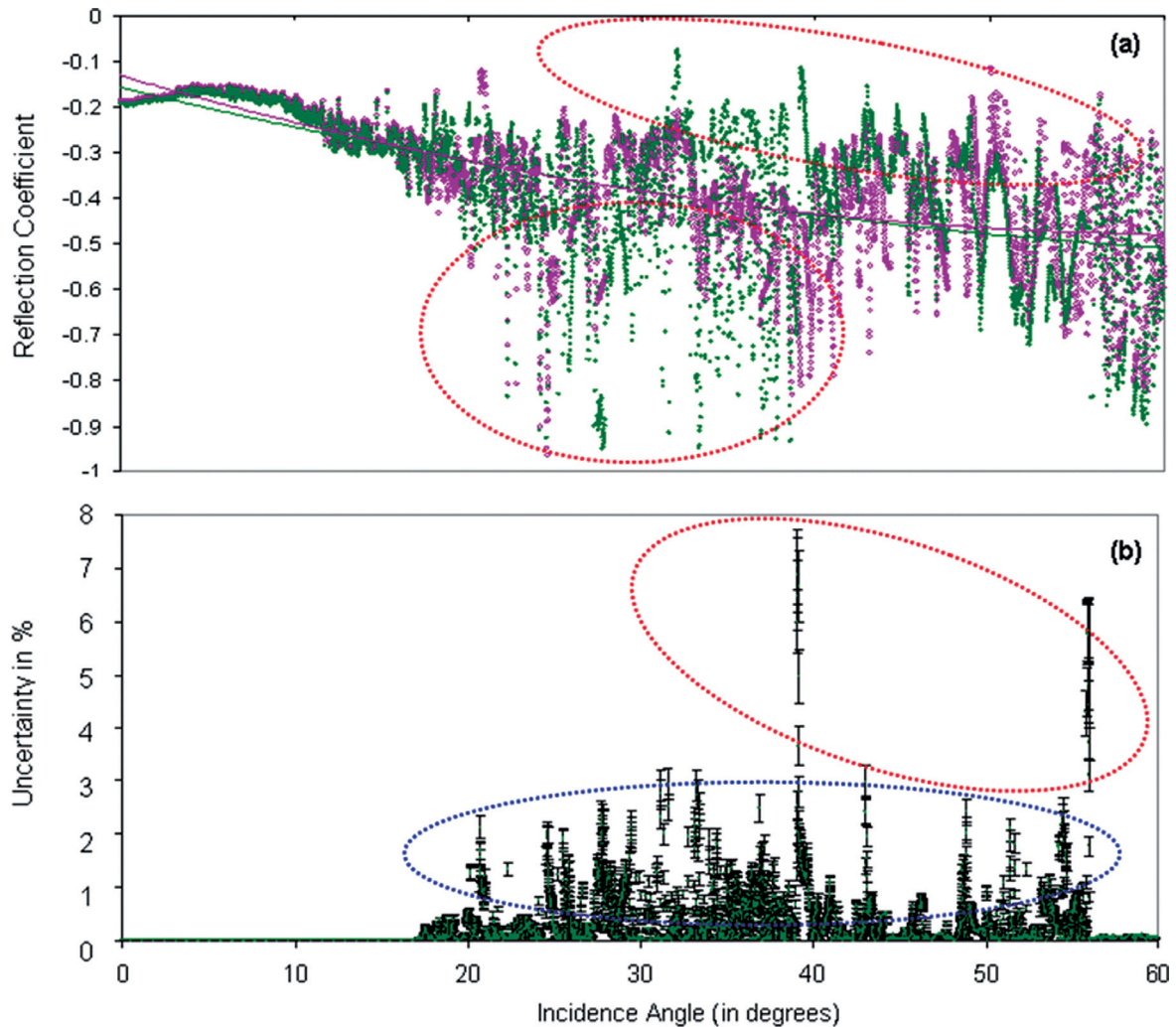
Figure 8
(a)Reflection Coefficient vs. Offset of the Modelled DBSR (Pink Dots) Using the Estimated Seismic Velocities from Figure 3 and the Real DBSR (Green Dots) Identified in GC Region Offshore USA, Showing a Negative Trend. The Least Square Polynomial Fit for Real (Green Line) and Modelled (Pink Line) Reflection Coefficients of the DBSR Correlate Well. Dotted Ovals Show the Scattered Data Points that are Caused by Structural Elements Discussed in the Text;
(b) Estimated Uncertainty in the Real and Modelled Values of Reflection Coefficients of the DBSR. The Maximum Uncertainty is 8%. The Blue Dotted Oval Shows that the Majority of Data Points Have Less than 3% Uncertainty. The Red Dotted Oval Shows Those Data Points with Uncertainty Between 3% and 8%.

To assess the reliability of AVO analysis in marine gas hydrate studies, the AVO response of BSRs is modelled. The scattering in the amplitude observed for both real and modelled BSRs (single and double BSR) appears to be caused by the vertical venting structures which are directly related to the 'plumbing mechanism' and may help explain the seepage of marine gases into atmosphere. The uncertainty estimation in the AVO response is in an acceptable range. The maximum uncertainty regions correspond to a large number of the gas vent structures whereas minimum uncertainty is observed when fewer venting structures are seen.
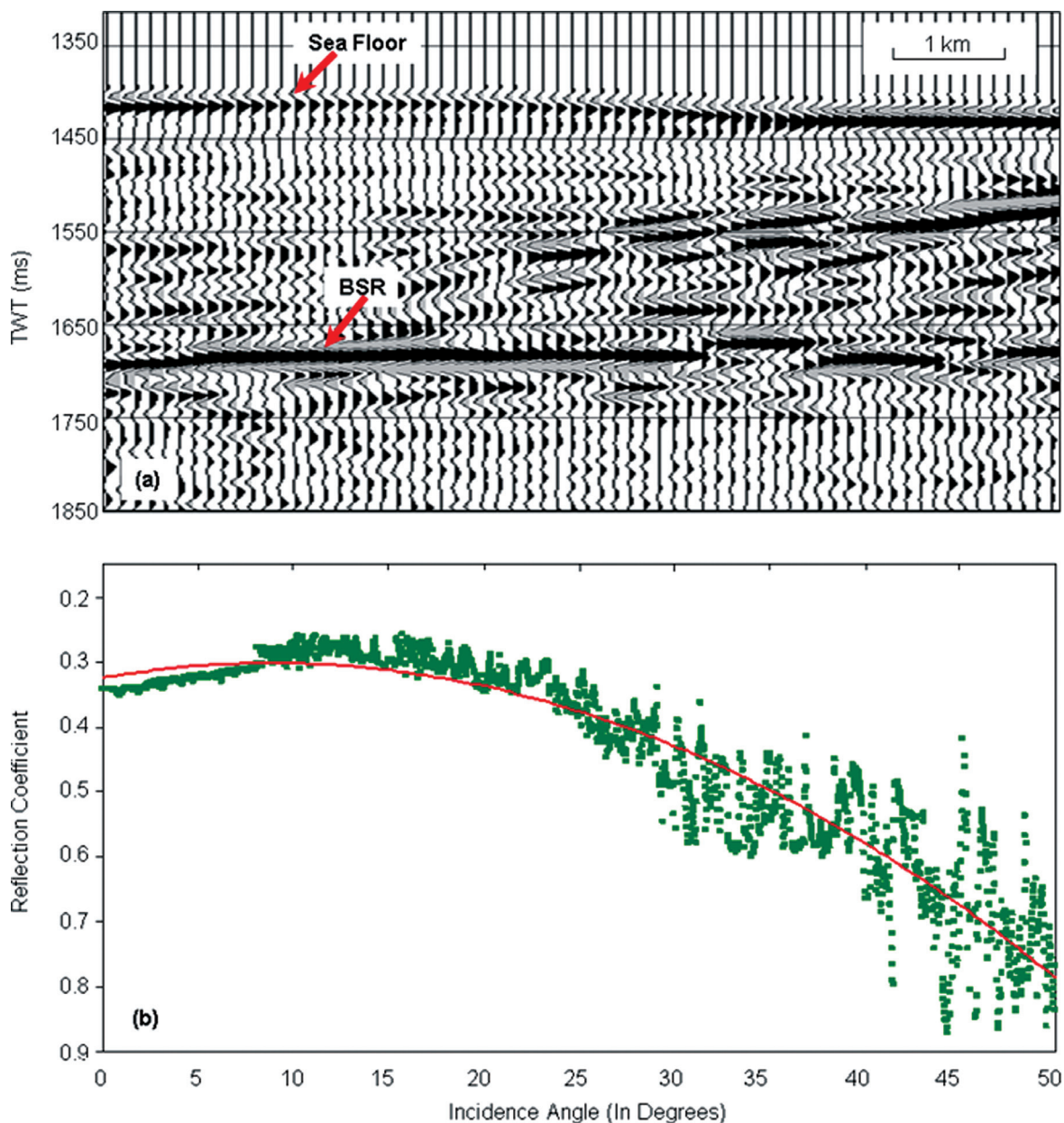
Figure 9
(a) Time Migrated Seismic Section from the Southern Part of the GC Region Where we Observed a Continuous BSR, Which is Showing the Negative Polarity with Respect to Sea Floor; (b) Reflection Coefficient of BSR Showing a Sharp Negative Trend Without much Amplitude Scattering

At this stage, to study the relationship between amplitude scattering and venting structures, we calculated the reflection coefficient of BSR at a location (further south) from the GC study area where we a see a continuous BSR and no gas venting structure (Figure 9). The reflection coefficient show a negative trend and a good fit for the data points is obtained. This exercise is repeated at a location where we see the gas venting structure and relatively low amplitude strength BSR (Figure 10). The reflection coefficient of a continuous BSR (Figure 9b) doesn't show amplitude scattering data point whereas the reflection coefficient of BSR where gas venting structure is evident (Figure 10b) represents amplitude scattering. Studying the behaviour of AVO trend at these two locations (Figures 9 and 10), it can be said that the amplitude scattering corresponds to the gas venting structure. The underlying zones of reduced reflection amplitude indicate the presence of gas, which migrates upward through near-vertical conduits to feed the vent structure. The local geology at the GC area and underlying plumbing system indicate a high flux of gases migrating through the region.
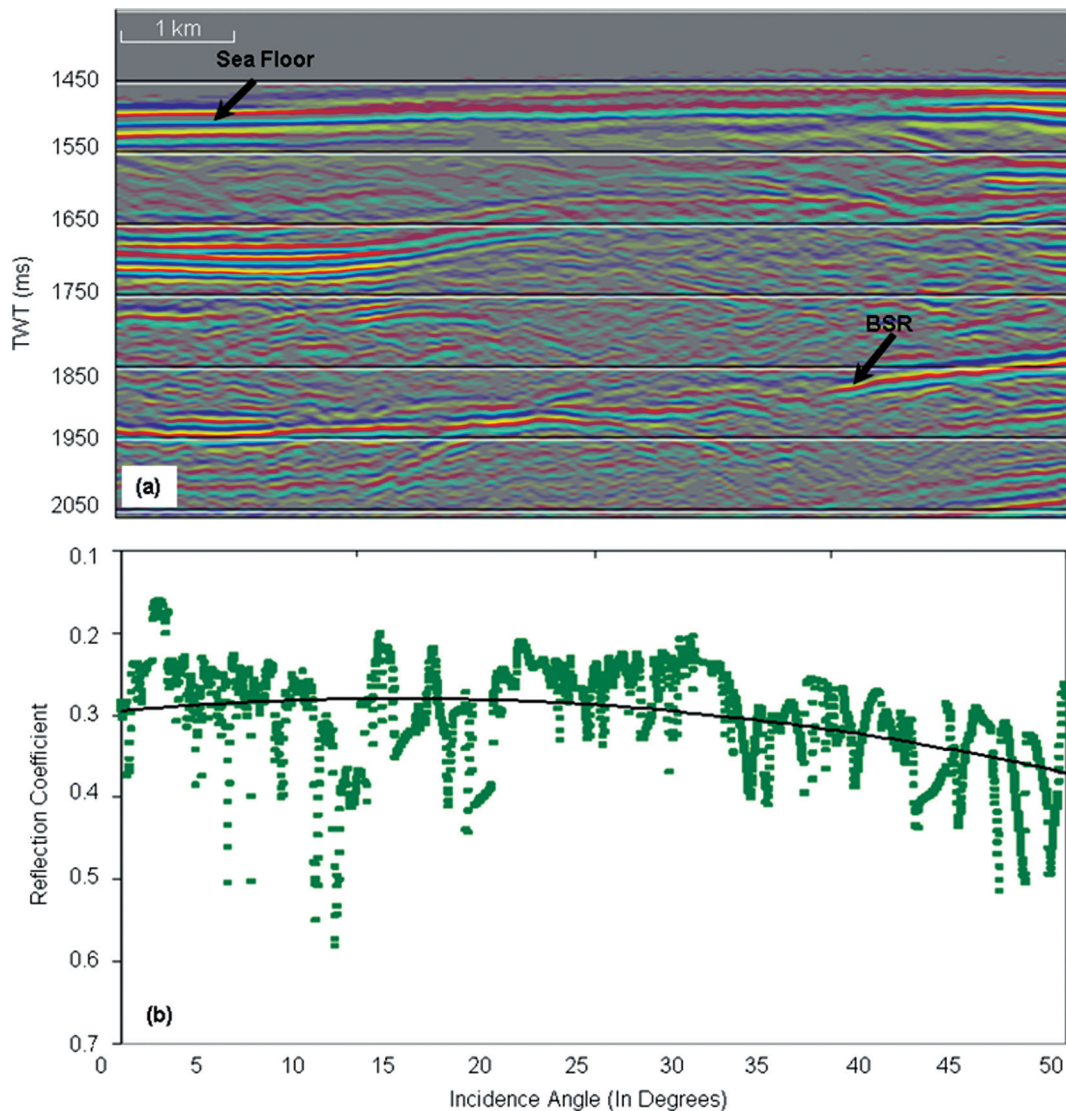
Figure 10
(a) Time Migrated Seismic Section over a Gas Venting Structure from the GC Region; (b) Reflection Coefficient of BSR Showing a Negative Trend with Amplitude Scattering

DISCUSSIONS AND CONCLUSIONS

Our interpretation of the seismic reflection data from KK basin and GC region indicates that dim zones up to >5km wide above the GHSZ contain relatively high velocities produced by the higher concentration of gas hydrates. Due to active vertical migration of gas to the sea floor within the stability conditions, thermogenic gas hydrates occur within the GC region. Huge amount of thermogenic gas hydrates occur in association with the outlets of hydrocarbon vents. The second example from GC region (Figure 2) show high velocities attributed to gas hydrate just beneath the sea bed and it appears the gases vent directly into the ocean. The example shows a high influx of upwelling gases connected to the deeper source zone of highly concentrated gas through a discrete network of steep fractures and faults. Gas hydrate is also rapidly precipitated in sea-floor experiments using natural vent gas as the starting material. One of the of experiments of this type is conducted by using thermogenic hydrocarbon gases as the starting material that vented to the water column in association with the sea-floor mounds of natural gas hydrate (Sassen and Macdonald, 1997). The seismic image from the hydrate mound and DBSR regions (Figures 2 and 3a) indicate that these structures are the result of a low flux of gas input from a diffuse region of the underlying structural elements. In both of the examples, the free gases migrated from deeper structures to feed the hydrate vents. There is a strong possibility of a salinity effect driven by the migrating gases as one of the principal mechanisms, allowing free gases to escape through the GHSZ in the high flux vent. In the mound and

DBSR structures of low flux, however, the gases escape through the seabed as a dissolved phase. The results reveal high and low flux styles of gas venting from adjacent, local systems several kilometres apart that appear to be good examples of 'seepage to leakage' and could help in explaining the complex plumbing system.

AVO analysis shows that the seepage-to-leakage mechanism appears to be linked to the amplitude variations of BSRs. The local scattering of the BSR seismic amplitudes is probably due to structural elements (vertical discrete fracture network, faults, vertical venting structures, hydrate mounds etc.) that are causing the seepage of underlying gases. Modelled BSR reflection coefficients in a realistic anisotropic medium can explain the variations observed in real data. This suggests that anisotropy is also contributing to the complexity of the seepage-to–leakage plumbing system. The lateral variability in the reflection strength may be due to the variation in hydrate concentration or due the variation in the amount of free gas beneath the hydrate. The hydrate may be distributed laterally in a discontinuous or disseminated layer. The uncertainty estimates are quite low and we gained confidence in our results. More sophisticated experiments from 4C data, permanent monitoring systems and research submarine platforms could significantly enhance our understanding of thermogenic gas hydrate formation in the deep sea.

ACKNOWLEDGEMENTS

REFERENCES

[1] Andreassen, K., Hogstead, K., & Berteussen, K. A. (1990). Gas Hydrate in the Southern Barents Sea, Indicated by a Shallow Anomaly. *First Break*, *8*(6), 235-245.

[2] Bangs, N. L., Musgrave, R. J., & Tréhu, A. M. (2005). Upward Shifts in the South Hydrate Ridge Gas Hydrate Stability Zone Following Post-Glacial Warming Offshore Oregon. *Journal of Geophysical Research*, *110*, B03102.

[3] Behura, J., & Tsvankin, I. (2009). Reflection Coefficients in Attenuative Anisotropic Media. *Geophysics*, *74*(5), WB193-WB202.

[4] Buffett, B. A., & Zatsepina, O. Y. (1999). Metastability of Gas Hydrate. *Geophysical Research Letters*, *26*, 2981–2984.

[5] Castagna, J. P., & Backus, M. M. (1993). *Offset-Dependent Reflectivity: Theory and Practice of AVO Analysis*. Tulsa, OK: Society of Exploration Geophysicists.

[6] Ecker, C., Dvorkin, J., & Nur, A. (1998). Sediments with Gas Hydrates: Internal Structure from Seismic AVO. *Geophysics*, *63*, 1659–1669.

[7] Golmshtok, A. Y., & Soloviev, V. A. (2006). Some Remarks on the Thermal Nature of the Double BSR. *Marine Geology*, *229*(3-4), 187-198.

[8] Gay, A., Lopez, M., Berndt, C., & Seranne, M. (2007). Geological Controls on Focused Fluid Flow Associated with Seafloor Seeps in the Lower Congo Basin. *Marine Geology*, *244*(1-4), 68–92.

[9] Gorman, A. R., Holbrook, Hornbach, W. S., Hackwith, M. J., Lizarralde, K. L. D., & Pecher, I. (2002). Migration of Methane Gas Through the Hydrate Stability Zone in a Low-Flux Hydrate Province. *Geology*, *30*(4), 327-330.

[10] Haacke, R. R., Hyndman, R. D., Park, K. P., Yoo, D. G., Stoian, I., & Schmidt, U. (2009). Migration and Venting of Deep Gases into the Ocean Through Hydrate-Choked Chimneys Offshore Korea. *Geology 37*(6), 531-534.

[11] Haacke, R. R., Westbrook, G. K., & Hyndman, R. D. (2007). Gas Hydrate, Fluid Flow and Free-Gas: Formation of the Bottom-Simulating Reflector. *Earth and Planetary Science Letters*, *261*, 407–420.

[12] Haacke, R. R., Westbrook, G. K., & Riley, M. S. (2008). Controls on the Formation and Stability of Gas Hydrate-Related Bottom-Simulating Reflectors (BSRs): A Case Study from the West Svalbard Continental Slope. *Journal of Geophysical Research*, *113*, B05104.

[13] Heggland, R. (1997). Detection of Gas Migration from a Deep Source by the Use of Exploration 3D Seismic Data, *Marine Geology*, *137*, 41-47.

[14] Henriet, J. P., & Mienert, J. (Eds.). (1998). *Gas Hydrates-Relevance to World Margin Stability and Climatic Change*. *Geological Society of London*, *Special Publication*, *137*, 338.

[15] Holbrook, W. S., Lizarralde, D., Pecher, I. A., Gorman, A. R., Hackwith, K. L., Hornbach, M., & Saffer, D. (2002). Escape of Methane Gas Through Sediment Waves in a Large Methane Hydrate Province. *Geology*, *30*, 467-470.

[16] Hovland, M., Gallagher, J. W., Clennell, M. B., & Lekvam, K. (1997). Gas Hydrate and Free Gas Volumes in Marine Sediments: Example from the Niger Delta Front. *Marine and Petroleum Geology*, *14*, 245-255.

[17] Hovland, M., & Svensen, H. (2006). Submarine Pingoes: Indicators of Shallow Gas Hydrates in a Pockmark at Nyegga, Norwegian Sea. *Marine Geology*, *228*, 15-23.

[18] Hyndman, R. D., & Spence, G. D. (1992). A Seismic Study of Methane Hydrate Marine Bottom Simulating Reflectors. *Journal of Geophysical Research*, *97*, 6683–6698.

[19] Hubbert, M. K., & Willis, D. G. W. (1957). Mechanics of Hydraulic Fracturing. *Trans. Am. Inst. Min. Eng.*, *210*, 153–168.

[20] Morley, C. K. (2003). Outcrop Examples of Mudstone Intrusions from the Jerudong Anticline, Brunei Darussalam and Inferences for Hydrocarbon Reservoirs. *Geological Society of London*, *Special Publication*, *216,* 381–392.

[21] Musgrave, R. J., Bangs, N. L., Larrasoaña, J. C., Gracia, E., Hollamby, J.A., & Vega, M.E. (2006). Rise of the Base of the Gas Hydrate Zone Since the Last Glacial Recorded by Rock Magnetism. *Geology*, *34*(2), 117-120.

[22] Nimblett, J., & Ruppel, C. (2003). Permeability Evolution During Formation of Gas Hydrates in Marine Sediments. *Journal of Geophysical Research*, *108*, B9.

[23] Ostrander, W. J. (1984). Plane wave reflection coefficients for gas sands at non normal angles of incidence. *Geophysics*, *49*, 1637-1648.

[24] Park, K. P. (2008). Gas Hydrate Exploration Activities in Korea. [Motion picture]. *Proceedings of the 6th International Conference on Gas Hydrates,* Vancouver.

[25] Paull, C. K., Ussler, W., III, Borowski, W. S., & Spiess, F. N. (1995). Methane-Rich Plumes on the Carolina Continental Rise: Associations with Gas Hydrates. *Geology*, *23*, 89-92.

[26] Pecher, I. A., Holbrook, W. A., Sen M. K., Lizarralde, D., Wood, W. T., Hutchinson, D. R., Dillon, W. P., Hoskins, H., & Stephen, R. A. (2003). Seismic Anisotropy in Gas-Hydrate and Gas Bearing Sediments on the Blake Ridge, from a Walk-Away Vertical Seismic Profile. *Geophysical Research Letters*, *30*(14), 1733.

[27] Posevang, J., & Mienert, J. (1999). The Enigma of Double BSRs: Indicators for Changes in the Hydrate Stability Field. *Geo Marine Letters*, *19*, 157–163.

[28] Rajput, S., Thakur, N. K., Rao, P. P., & Joshi, A. (2010). AVO Response for a Complex Double Bottom Simulating Reflectors Model. *Current Science*, *98* (10), 1354-1358.

[29] Rajput, S. (2009). *Analysis of Ocean Bottom Seismometer Data for Gas Hydrate Studies and Subsurface Models* (Doctoral dissertation). Kurukshetra University, Kurukshetra.

[30] Riedel, M., Collett, T. S., Malone, M. J., & the Expedition 311 Scientists. (2006). Cascadia Margin Gas Hydrates. *Proc. IODP*, *311*.

[31] Rueger, A. (1996). *Reflection Coefficients and Azimuthal AVO Analysis in Anisotropic Media* (Doctoral dissertation). Colorado School of Mines, Golden.

[32] Santoso, D., Alfian, Alam, S., Sulistiyono, Hendrajaya, L. & Munadi, S. (1995). Estimation of Limestone Reservoir Porosity by Seismic Attribute and AVO Analysis. *Exploration Geophysics*, *26*, 437-443.

[33] Sassen, R., & MacDonald, I. R. (1997). Hydrocarbons of Experimental and Natural Gas Hydrates: Gulf of Mexico Continental Slope. *Organic Geochemistry*, *26*, 289–293.

[34] Shipley, T. H., Houston, M. H., Buffler, R. T., Shaub, F. J., McMillen, K. J., Ladd, J. W., & Worzel, J. L. (1979). Seismic Evidence for Widespread Possible Gas Hydrate Horizons on Continental Slopes and Rises. *American Association of Petroleum Geologists Bulletin*, *63*, 2204–2213.

[35] Sloan, E. D. (1998). *Clathrate Hydrates of Natural Gases*. New York: Marcel Decker.

[36] Suess, E., Torres, M. E., Bohrmann, G., Collier, R. W., Greinert, J., Linke, P., Rehder, G., Trehu, A., Wallmann, K., Winckler, G., & Zuleger, E. (1999). Gas Hydrate Destabilization: Enhanced Dewatering, Benthic Material Turnover and Large Methane Plumes at the Cascadia Margin. *Earth and Planetary Science Letters*, *170*, 1–15.

[37] Thakur, N. K., & Rajput, S. (2010). *Exploration of Gas Hydrates Geophysical Techniques*. New York: Springer Publications.

[38] Tingay, M. R. P., Hillis, R., Morley, C. K., Swarbrick, R. E., & Okpere, E. C. (2003). Pore Pressure/Stress Coupling in Brunei Darussalam-Implications for Shale Injection, in Subsurface Sediment Mobilization (Edited by P. Van Rensbergen *et al*.). *Geological Society of London, Special. Publication*, *216*, 369 – 379.

[39] Tréhu, A. M., Lin, G., Maxwell, E., & Goldfinger, C. (1995). A Seismic Reflection Profile Across the Cascadia Subduction Zone Offshore Central Oregon: New Constraints on the Deep Crustal Structure and on the Distribution of Methane in the Accretionary Prism. *Journal of Geophysical Research*, *100*(B8), 15,101-15,116.

[40] Trehu, A. M., Torres, M. E., Moore, G. F., Suess, E., & Bohrmann, G. (1999). Temporal and Spatial Evolution of a Gas Hydrate-Bearing Accretionary Ridge on the Oregon Continental Margin. *Geology*, *27*, 939-942.

[41] Tsvankin, I. (2005). *Seismic Signatures and Analysis of Reflection Data in Anisotropic Media*. Netherlands: Elsevier Science.

[42] Wood, W. T., Gettrust, J. F., Chapman, N. R., Spence, G. D., & Hyndman, R. D. (2002). Decreased Stability of Methane Hydrates in Marine Sediments Owing to Phase-Boundary Roughness. *Nature*, *420*, 656-660.

[43] Zhang, Z., Han, D., & Yao, Q. (2011). Quantitative Interpretation for Gas Hydrate Accumulation in the Eastern Green Canyon Area, Gulf of Mexico Using Seismic Inversion and Rock Physics Transform. *Geophysics*, *76*(B139).

[44] Zoeppritz, K. (1919). *Erdbebenwellen VIII B On the Reflection and Penetration of Seismic Waves Through Unstable Layers*. *Goettinger Nachrichten*, *1*, 66-84.

[45] Zuhlsdorff, L., & Spiess, V. (2004). Three-Dimensional Seismic Characterization of a Venting Site Reveals Compelling Indications of Natural Hydraulic Fracturing. *Geology*, *32*(2), 101-104.